Image Mem-Processing Bio-Inspired Cellular Arrays with Bistable and Analogue Dynamic Memristors

A. Ascoli, I. Messaris, R. Tetzlaff
Institute of Circuits and Systems
Technische Universität Dresden

S. Kang
Jack Baskin School of Engineering
University of California Santa Cruz

L.O. Chua
Department of Electrical Engineering and
Computer Sciences, University of California

***Abstract*—By introducing memristors into circuit design, the limitations of traditional purely-CMOS hardware may be overcome. However, an extension of standard techniques for the analysis and design of conventional computing structures may be necessary to allow their applicability to the memristive counterparts. This paper adopts a generalization of the Dynamic Route Map system-theoretic concept to elucidate the mechanisms by which bio-inspired arrays of locally-coupled circuits, employing memristors with either bistable-like or analogue dynamic switching behaviours, accomplish image mem-processing tasks through the dynamical evolution of their states toward predefined equilibria.**

I. Introduction

A robust bio-inspired multivariate signal processing framework, particularly suitable for the solution of time-critical problems, and, therefore, of special appeal to Internet-of-Things (IoT) applications, is the well-known *Cellular Nonlinear Network* (CNN) paradigm [1]. In its simplest form, a CNN consists of a rectangular lattice of regularly-spaced identical locally-coupled dynamic processors, known as cells, each of which processes information through the analogue dynamics of its state. Despite each processing element is physically coupled only to its closest neighbors within a prescribed sphere of influence, the effects of the analogue behaviour of its state may propagate from cell to cell throughout the network. The local connectivity simplifies the architecture of a CNN in comparison with a Hopfield network, and further endows the bio-inspired array with a massively-parallel computing power. These benefits have motivated the use of CNNs in combination with matrices of sensors for the development of powerful arrays [2], capable to combine sensing [3] and computing [4] functionalities within a unique physical medium, allowing the real-time solution of numerous problems in various sectors, including the medical, military, and industrial fields [5]. In order to endow the CNN with stored programmability on board, each cell accommodates additional memory units. The locally-distributed memory provides the overall engine with a truly non-von Neumann computing architecture. The price to pay in the design of this Universal Machine [6] is associated to the necessity to allocate a large integrated circuit (IC) area to the memory bank in each processing element. This limits the maximum spatial resolution, which is currently achievable in the aforementioned class of sensor-processor arrays [2]. The disruptive memristor technology [7] may be the key to extend and/or complement the functionalities of state-of-the-art purely-CMOS circuits and systems. With reference to CNN design, the adoption of memristors [8], featuring the peculiar ability to store or process data within a single nanoscale volume, for the development of an innovative circuit implementation of the basic processing element may obviate the necessity to include extra memory units in each cell, allowing to shrink considerably its size as compared to the standard hardware realization, and paving the way toward the future fabrication of miniaturized, lightweight, and low-power technical systems with unprecedented data acquisition, storage and processing functionalities on board. Given the promising potential of bio-inspired memristive cellular structures, it is worth to devote efforts to develop system-theoretic techniques enabling the exploration of the main factors underlying their operation, the identification and circumvention of potential drawbacks, as well as the development of programmability strategies for a robust accomplishment of a given memcomputing task. In fact, the introduction of memristors in circuit design calls for the generalization of traditional techniques for the analysis and synthesis of conventional electrical and electronic systems. Let us gain a deeper insight into this important aspect, focusing on the class of nonlinear dynamic arrays under focus. Including a first-order non-volatile [9] memristor in parallel to the capacitor in the classical circuit implementation of each processing element of a standard space-invariant CNN [1], as shown in Fig. 1, the resulting bio-inspired array is referred to as Memristor CNN (M-CNN). The dynamical

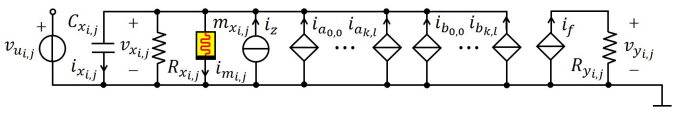

Figure 1. Circuit implementation of a $M \times N$ M-CNN cell $C(i,j)$, where $i \in \{1,\ldots,M\}$, and $j \in \{1,\ldots,N\}$.

evolution of the state of a standard CNN cell, namely the voltage $v_{x_{i,j}}$ across its capacitor $C_{x_{i,j}}$, may be inferred, for any initial condition $v_{x_{i,j}}(0)$/input voltage $v_{u_{i,j}}$ combination, by inspecting the particular $\dot{v}_{x_{i,j}}$–$v_{x_{i,j}}$ locus, which foliates from the cell Dynamic Route Map[1] (DRM) [1] under a given circuit parameter setting. However, a generalization of this tool is necessary for the investigation of the operating principles of a M-CNN cell [10]. Specifically, depending upon the memristor employed in the cell circuit, two scenarios are possible:

1) In case the memristor may only undergo abrupt

[1]A cell Dynamic Route Map [8] is a family of $\dot{v}_{x_{i,j}}$–$v_{x_{i,j}}$ loci, each of which is obtained upon assignment of a certain value to a control variable, while all other circuit parameters are kept unchanged. The time evolution of the capacitor voltage may be easily evinced by inspecting a locus of this kind: wherever $\dot{v}_{x_{i,j}}$ has positive (negative) sign, $v_{x_{i,j}}$ increases (decreases) with time.

switching transistions between a high and a low resistive state under voltage excitation, acting essentially as a bistable-like device, the M-CNN cell may be approximated at any given time as one of two admissible first-order dynamic systems, each of which is associated to one of the two possible memristor states. In these circumstances, under a fixed circuit parameter setting, the dynamic evolution of the capacitor voltage $v_{x_{i,j}}$ is governed at any given time by one of two possible $\dot{v}_{x_{i,j}}$–$v_{x_{i,j}}$ loci, depending upon the resistive state the memristor sits in. To provide some evidence for the richer dynamics a bistable-like memristor endows the cell with, it is sufficient to note that the transition from one of the two loci to the other one may allow the motion of the capacitor voltage $v_{x_{i,j}}$ toward an equilibrium $\bar{v}_{x_{i,j}}$, which a standard CNN cell may not admit [10].

2) In case the memristor resistance may be finely tuned upon suitable stimulation, the M-CNN cell is a dynamic system with two degrees of freedom. As a result, the DRM graphic tool, applicable to first-order ordinary differential equations (ODEs) only, cannot be used to gain some insight into the operating principles of the bio-inspired array. In this case it is necessary to consider a generalization of this system-theoretic concept, introducing the Second-Order Dynamic Route Map[2] (DRM_2). The basic component of the DRM_2 graphical tool, constituting the equivalent of a $\dot{v}_{x_{i,j}}$–$v_{x_{i,j}}$ locus for the standard DRM, and called State Dynamic Portrait (SDP), illustrates how the signs of the two state variables of the second-order cell – namely the memristor state $x_{m_{i,j}}$, and the capacitor voltage $v_{x_{i,j}}$ – change throughout the two-dimensional state space under a given circuit parameter setting, allowing to determine the path followed by a trajectory from any initial condition $(x_{m_{i,j}}(0), v_{x_{i,j}}(0)$ as it approaches a relevant equilibrium $(\bar{x}_{m_{i,j}}, \bar{v}_{x_{i,j}})$.

This manuscript shows how, extending the classical DRM technique according to the aforementioned guidelines on the basis of the nature of the memristor switching behavior[3], enables to understand thoroughly the mechanisms, by which a M-CNN may accomplish a fundamental image processing operation through the time evolution of its dynamic states toward predefined equilibria. It is worth pointing out that the system-theoretic tools, which in this paper are employed to investigate the nonlinear dynamics of M-CNN cells with bistable-like or analog dynamic memristors, may in general be applied to any electronic system, including a memristive device, that can be modelled by a first- or second-order ODE set, respectively.

II. M-CNN CLASS

With $i \in \{1, \ldots, M\}$, and $j \in \{1, \ldots, N\}$, the second-order ODE modelling a M-CNN from the proposed class[4] is

$$\dot{x}_{m_{i,j}} = k(v_{x_{i,j}}) \cdot \big(\text{step}(v_{x_{i,j}}) \cdot f_+^p(x_{m_{i,j}}) + \text{step}(-v_{x_{i,j}}) \cdot f_-^p(x_{m_{i,j}})\big), \quad (1)$$

$$\dot{v}_{x_{i,j}} = \frac{-G_x \cdot v_{x_{i,j}} - i_{m_{i,j}} + i_{a_{0,0}}}{C_x} + \frac{i_{w_{i,j}}}{C_x}, \quad (2)$$

where equation (1) ((2)) governs the time evolution of the memristor state $x_{m_{i,j}}$ (the capacitor voltage $v_{x_{i,j}}$). Together with the first cell ODE equation, where $\text{step}(\cdot)$ denotes the Heaviside function, the formula for the current through the memristor $m_{x_{i,j}}$, expressed via a Ohm-based law as

$$i_{m_{i,j}} = G(x_{m_{i,j}}) \cdot v_{m_{i,j}}, \quad (3)$$

in which

$$G(x_{m_{i,j}}) = x_{m_{i,j}}^{-1}, \quad (4)$$

and $v_{m_{i,j}}$ stand for the memristor conductance and voltage, respectively, represents the mathematical description of a first-order voltage-controlled non-volatile generic [11] memristor with restricted memory state existence domain[5], as proposed by Pershin and Di Ventra in [12] to characterize the memristive dynamics of a number of physical nanostructures [13]. Given that the state evolution function in equation (1) is *anti-sign invariant* [8], as follows from the expression for $k(v_{x_{i,j}})$, reading as

$$k(v_{x_{i,j}}) = -\beta \cdot v_{x_{i,j}} + (\beta - \alpha) \cdot \frac{|v_{x_{i,j}} + V_t| - |v_{x_{i,j}} - V_t|}{2}, \quad (5)$$

where $\alpha \mathbb{R}_{>=0}\, \Omega \cdot \text{V}^{-1} \cdot \text{s}^{-1}$ $(\beta > \alpha)$ denotes the slope $k'(v_{x_{i,j}})$ of the piecewise-linear characteristic (5) for $|v_{x_{i,j}}| \leq (>) V_t$, with $V_t \in \mathbb{R}_{>0}$ standing for the threshold voltage for memristor switching, the introduction of the continuous and differentiable boundary condition window [14]

$$f_\star^p(x_{m_{i,j}}) = 1 - \left((x_{m_{i,j}} - x_{on}) \cdot (x_{off} - x_{on})^{-1} + \xi\right)^{2 \cdot p}, \quad (6)$$

where $\xi = -1\,(0)$ if $\star = +\,(-)$, whereas $p \in \mathbb{Z}_{>0}$, into the memristor state equation (1) prevents the memristor state from ever decreasing below (increasing above) its lower (upper) bound x_{on} (x_{off}). The cell capacitor current is the sum of two main components, as realizable from equation (2). The first component consists of a series of three terms, each of which is a function of at least one of the two cell states, more specifically the currents flowing out of the capacitor into the linear resistor of conductance $G_x = R_x^{-1}$, and into the memristor, respectively, and the current $i_{a_{0,0}} = a_{0,0} \cdot v_{y_{i,j}}$ injected into the capacitor, modulated by the *self-feedback synaptic weight* $a_{0,0}$ [1], and controlled by the cell output voltage $v_{y_{i,j}}$, expressed by

$$v_{y_{i,j}} = R_y \cdot i_f(v_{x_{i,j}}), \text{where} \quad (7)$$

$$i_f(v_{x_{i,j}}) = g_{lin} \cdot R_y \cdot f(v_{x_{i,j}}), \quad (8)$$

[2] A cell Second-Order Dynamic Route Map represents a family of State Dynamic Portraits, each of which is associated to a certain value for a control variable, while all other circuit parameters are kept unchanged. The time evolution of a trajectory point $(x_{m_{i,j}}, v_{x_{i,j}})$ may be easily inferred by inspecting a State Dynamic Portrait: wherever $\dot{x}_{m_{i,j}}$ and/or $\dot{v}_{x_{i,j}}$ has positive (negative) sign, $x_{m_{i,j}}$ and/or $v_{x_{i,j}}$ increases (decreases) with time.

[3] Depending upon the physical realization of the memristor device, and on the circuit and stimuli, which accommodates and excite it, respectively, its response may be characterized by abrupt switching between a lower and an upper resistive state, or by smooth memristance modulation across the whole allowable resistance range.

[4] With reference to Fig. 1, the capacitance of the cell capacitor satisfies $C_{x_{i,j}} = C_x \in \mathbb{R}_{>0}$, the resistance of the resistor in parallel to the memristor meets the constraint $R_{x_{i,j}} = R_x \in \mathbb{R}_{>0}$, and the resistance of the output stage resistor is chosen in such a way that $R_{y_{i,j}} = R_y \in \mathbb{R}_{>0}$ for all $i \in \{1, \ldots, M\}$ and for all $j \in \{1, \ldots, N\}$, given that the M-CNN cells are assumed to be identical one to the other.

[5] The memory state $x_{m_{i,j}}$ in the Pershin and Di Ventra differential algebraic equation (DAE) set [12], expressed by equations (1), (3), and (4), is constrained to lie at all times within the closed set $\mathcal{D} \triangleq [x_{on}, x_{off}]$, where x_{on} (x_{off}) represents the largest (smallest) possible memristor resistance.

$g_{lin} \in \mathbb{R}_{>0}$ is a conductance parameter, while

$$f(v_{x_{i,j}}) = \frac{|v_{x_{i,j}} + v_{sat}| - |v_{x_{i,j}} - v_{sat}|}{2} \tag{9}$$

is known as *standard output nonlinearity* [1], where $v_{sat} \in \mathbb{R}_{>0}$ is the so-called saturation voltage[6]. Referring once more to equation (2), the second component of the cell capacitor current, called *offset current*, is expressed by

$$i_{w_{i,j}} = i_{b_{0,0}} + \sum_{\substack{k,l=-1 \\ (k,l)\neq(0,0)}}^{1} \left(i_{a_{k,l}} + i_{b_{k,l}}\right) + i_z, \tag{10}$$

where, looking at Fig. 1 for the circuit interpretation, $i_{b_{0,0}} = b_{0,0} \cdot v_{u_{i,j}}$ denotes the self-feedforward synaptic current, modulated by the *self-feedforward synaptic weight* $b_{0,0}$ [1], and controlled by the cell input voltage $v_{u_{i,j}}$, $i_{b_{k,l}} = b_{k,l} \cdot v_{u_{i+k,j+l}}$ ($i_{a_{k,l}} = a_{k,l} \cdot v_{y_{i+k,j+l}}$) stands for the feedforward (feedback) synaptic current, modulated by the *feedforward (feedback)) synaptic weight* $b_{k,l}$ ($a_{k,l}$) [1], and controlled by the input (output) voltage $v_{u_{i+k,j+l}}$ ($v_{y_{i+k,j+l}}$) of the neighboring cell $C(i+k, j+l)$, with $k, l \in \{1, 0, 1\}$ such that $(k, l) \neq (0, 0)$, whereas $i_z = I \cdot z$ represents the threshold current, with z symbolising the *threshold* [1], and I a dimensionless constant. The generalization of the system-theoretic DRM graphic tool [1], discussed in section I, is adopted in sections III and IV to gain a deep insight into the operating principles of a M-CNN from the proposed class, as it accomplishes a fundamental image processing operation, under the hypothesis that the memristors employed in the processing elements feature bistable-like and analogue dynamic behaviours, respectively. The cell circuit parameters, which are kept unchanged in the remainder of this manuscript, are: $V_t = 0.8\,\mathrm{V}$, $x_{on} = 2\,\mathrm{k\Omega}$, $x_{off} = 10\,\mathrm{k\Omega}$, $p = 40$, $g_{lin} = 1\,\mathrm{m\Omega^{-1}}$, $R_y = 1\,\mathrm{k\Omega}$, $v_{sat} = 0.1\,\mathrm{V}$, and $I = 1$.

III. Image Processing in Bio-Inspired Arrays with Bistable-like Memristors

Assuming that the memristor may only experience abrupt switching transitions[7] between two possible resistive states upon excitation, the cell model may be approximately described at any given time by the first-order equation (2), in which the memristor state $x_{m_{i,j}}$, to be inserted in the expression of equation (4) for the memductance, is fixed either to x_{off} or to x_{on}, similarly as it would happen at an equilibrium $\bar{x}_{m_{i,j}}$ of equation (1). While the DRM system-theoretic technique holds true for the analysis of the first-order cell model approximation, rewritten for the sake of simplicity below,

$$\dot{v}_{x_{i,j}} = \frac{-G_x \cdot v_{x_{i,j}} - \bar{x}_{m_{i,j}}^{-1} \cdot v_{x_{i,j}} + i_{a_{0,0}}}{C_x} + \frac{i_{w_{i,j}}}{C_x}, \tag{11}$$

where $i \in \{1, \ldots, M\}$, $j \in \{1, \ldots, N\}$, and $\bar{x}_{m_{i,j}} \in \{x_{on}, x_{off}\}$, differently from what occurs in a standard space-invariant CNN, for a certain cell circuit parameter setting, the one-dimensional state $v_{x_{i,j}}$ of a memristive processing element may evolve at any given time as specified by one of two possible $\dot{v}_{x_{i,j}}$–$v_{x_{i,j}}$ loci, depending upon the resistive state the cell memristor sits in, as anticipated in section II. The directed locus – with arrows pointing toward the west (east) on the $v_{x_{i,j}}$–$\dot{v}_{x_{i,j}}$ plane lower (upper) half – dictating the time evolution of the cell state whenever the memristor sits in the largest x_{off} (smallest x_{on}) possible resistive state, and called *Off (On) State Dynamic Route* $\mathrm{SDR_{off}}$ ($\mathrm{SDR_{on}}$), are highlighted in red (blue) throughout the paper. The *bistability condition*, according to which the output voltage $v_{y_{i,j}}$ of a completely stable [8] M-CNN cell $C(i, j)$ attains either of the two saturation levels $\pm v_{sat}$ at steady state[9] is given by [10]

$$a_{0,0} > R_y^{-1} \cdot g_{lin}^{-1} \cdot (\bar{x}_{m_{i,j}}^{-1} + G_x), \tag{12}$$

where $\bar{x}_{m_{i,j}}$ is set to x_{on} or to x_{off} depending upon the memristor resistive state. Importantly, since (12) imposes a higher lower bound for the self-feedback synaptic weight $a_{0,0}$ when the memristor features the on resistance, the bistability of a M-CNN processing element may be described in one of three possible ways:

1) A cell is found to be monostable irrespective of the memristor state, provided $a_{0,0} < R_y^{-1} \cdot g_{lin}^{-1} \cdot x_{off}^{-1}$.

2) A cell is found to be bistable when the memristor sits in the off state, while it features monostability when the memristor sits in the on state, provided $R_y^{-1} \cdot g_{lin}^{-1} \cdot x_{off}^{-1} < a_{0,0} < R_y^{-1} \cdot g_{lin}^{-1} \cdot x_{on}^{-1}$.

3) A cell is found to be bistable irrespective of the memristor state, provided $a_{0,0} > R_y^{-1} \cdot g_{lin}^{-1} \cdot x_{on}^{-1}$.

A M-CNN cell may thus feature a much richer nonlinear dynamics than a standard space-invariant CNN processing element [10]. To provide a hint on the potential of the memristor to widen the spectrum of functionalities of a cell, it is sufficient to observe that the existence of two possible state evolution functions, as expressed by the right hand side of equation (11), where $\bar{x}_{m_{i,j}}$ is set to x_{on} or to x_{off}, depending upon the memristor resistive state, may allow to synthesise a single 19-parameter gene [1] $\{\{a_{k,l}\}, \{b_{k,l}\}, z\}$, $k, l \in \{-1, 0, 1\}$, which allows the cell to accomplish either a pair of tasks simultaneously, or one of two distinct tasks, depending upon the memristor resistive state. This double functionality, which would be impossible for a standard space-invariant CNN processing element [1], stems from the fact that the M-CNN memcomputing paradigm is based upon the evolution of the states of all cells toward pre-defined equilibria, and that, in general, the $\dot{v}_{x_{i,j}}$–$v_{x_{i,j}}$ loci, associated to the memristor off and on state, respectively, admit a distinct number of equilibria, located in unequal locations and featuring different stability properties. Importantly, the observation of a sharp

[6] Importantly, combining equations (7), (8), and (9), the cell output voltage $v_{y_{i,j}}$ is found to attain the negative (positive) saturation voltage $-(+)v_{sat}$ over the domain $v_{x_{i,j}} < (>) - (+)v_{sat}$, known as *negative (positive) saturation region* [1], while it is identically equal to the cell capacitor voltage $v_{x_{i,j}}$ over the domain $|v_{x_{i,j}}| \leq v_{sat}$, known as *linear region* [1].

[7] Setting the capacitance of the cell capacitor to $C_x = 100\,\mathrm{nF}$, assigning the coefficients α and β in the formula (5) for the piecewise-linear nonlinearity $k(v_{x_{i,j}})$ the values $0\,\Omega \cdot \mathrm{V}^{-1} \cdot \mathrm{s}^{-1}$, and $10^{15}\,\Omega \cdot \mathrm{V}^{-1} \cdot \mathrm{s}^{-1}$, respectively, the memristor is found to exhibit at any given time either the on x_{on} or the off x_{off} resistance, unless it undergoes a practically instantaneous switching transition from one of the two states to the other one [10].

[8] Provided the hypotheses of the M-CNN complete stability criterion ([1], [15], [16], [17]) are satisfied, for any initial condition $v_{x_{i,j}}(0)$, the cell state $v_{x_{i,j}}$ converges toward an isolated equilibrium $\bar{v}_{x_{i,j}}$ as time goes to infinity. If, additionally, the bistability condition holds true, $\bar{v}_{x_{i,j}}$ is always found to reside in one of the two saturation regions, otherwise it may lie in the linear region.

[9] The cell output voltage $v_{y_{i,j}}$ of a completely stable M-CNN is said to be at steady state from the time instant $t_{i,j}^{(s)}$, at which the capacitor voltage $v_{x_{i,j}}$ enters either of the two saturation regions of the standard output nonlinearity of equation (9).

change in the path, followed by the cell state over time, from the directed off (on) memristor-based $\dot{v}_{x_{i,j}}$–$v_{x_{i,j}}$ locus, i.e. SDR_{off} (SDR_{on}), to the directed on (off) memristor-based $\dot{v}_{x_{i,j}}$–$v_{x_{i,j}}$ locus, i.e. SDR_{on} (SDR_{off}), is possible only when the capacitor voltage $v_{x_{i,j}}$ increases above (decreases below) the positive (negative) threshold voltage $+(-)V_t$. Furthermore, the introduction of a specific constant voltage stimulus in a particular location of the M-CNN cell may contribute to differentiate the on and off memristor-based $\dot{v}_{x_{i,j}}$–$v_{x_{i,j}}$ loci in terms of number, location, and stability nature of the equilibria, improving the robustness of the multi-purpose memcomputing paradigm. Let us apply these theoretical concepts to elucidate how a M-CNN with bistable-like memristors carries out a fundamental image processing task.

A. Binary Image Edge Extraction through a M-CNN with Bistable-like Memristors

The EDGE M-CNN is an *uncoupled non-autonomous*[10] memristive cellular array, which extracts edges from an input binary image. The set of *local rules*[11], that each processing element and its 8 direct neighbors are requested to obey to accomplish this task is reported in Table I.

Table I. LOCAL RULES APPLYING IN THE 3×3 NEIGHBORHOOD OF EACH EDGE M-CNN CELL $C(i,j)$.

local rule	$v_{u_{i,j}}$ / V	$v_{y_{i,j}}(t_{i,j}^{(s)})$	conditions on n_B
1	-1	$-v_{sat}$	irrespective of n_B
2	$+1$	$-v_{sat}$	if $n_B = 8$
3	$+1$	$+v_{sat}$	if $n_B \leq 7$

Choosing[12] $R_x = 10\,\text{M}\Omega$, and $a_{0,0} = 1.5 \cdot 10^{-3}\,\Omega^{-1}$, and recalling the bistability condition (12), the M-CNN cell is found to be bistable irrespective of the memristor resistive state $\bar{x}_{m_{i,j}} \in \{x_{on}, x_{off}\}$. Defining $b_{k,l} \triangleq b$ for all $k,l \in \{-1,0,1\}$ except for $(k,l) = (0,0)$, the offset current (10) may be recast as

$$i_{w_{i,j}} = b_{0,0} \cdot v_{u_{i,j}} + (2 \cdot n_B - 8) \cdot b\,\text{V} + I \cdot z, \tag{13}$$

where $n_B \in \{0,1,2,3,4,5,6,7,8\}$ defines how many of the 8 direct neighbors $\{C(i+k, j+l)\}$ have positive one input voltage $v_{u_{i+k,j+l}}$, $k,l \in \{-1,0,1\}$, $(k,l) \neq (0,0)$. Let us assign the values $9.2 \cdot 10^{-5}\,\Omega^{-1}$, $-1.15 \cdot 10^{-5}\,\Omega^{-1}$ and $-1.15 \cdot 10^{-5}$ to $b_{0,0}$, b, and z, respectively. Setting $x_{m_{i,j}}(0) = x_{on}$ and $v_{x_{i,j}} = 0\,\text{V}$, the capacitor voltage is found to evolve on the directed on memristor-based $\dot{v}_{x_{i,j}}$–$v_{x_{i,j}}$ locus, i.e. SDR_{on}, in each scenario of any rule[13] Particularly, in case $v_{u_{i,j}} = -1\,\text{V}$, as demonstrated in plot (a) of Fig. 2, irrespective of the value of n_B, $v_{x_{i,j}}$ decreases with time as it approaches an equilibrium located in the negative saturation region, implying $v_{y_{i,j}}(t_{i,j}^{(s)}) = -1\,\text{V}$, as requested by local rule 1. In case

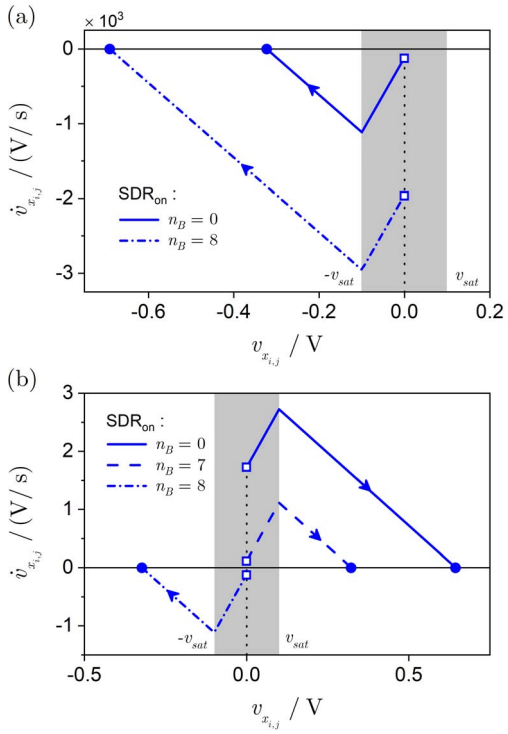

Figure 2. (a) ((b)) Cell SDR_{on} under $v_{u_{i,j}} = -1(+1)\,\text{V}$ for the limiting cases $n_B \in \{0,8\}(\{0,7,8\})$. The initial condition $v_{x_{i,j}}(0)$ is highlighted through a hollow square. A stable equilibrium is marked by means of a filled circle. The linear region $|v_{x_{i,j}}| \leq v_{sat}$ is indicated via a gray-shaded area.

$v_{u_{i,j}} = +1\text{V}$, equation (13) implies the negative (positive) sign for $i_{w_{i,j}}$ under $n_B = 8$ ($n_B \leq 7$). As illustrated in plot (b) of Fig. 2, it follows that in the first (latter) case the capacitor voltage decreases (increases) with time, converging toward an equilibrium located within the negative (positive) saturation region, where $v_{y_{i,j}}(t_{i,j}^{(s)}) = -(+)1\,\text{V}$, as requested by rule 2 (3). Let us now choose different values for R_x, $a_{0,0}$, b, $b_{0,0}$, and z, specifically $1\,\text{k}\Omega$, $2.3 \cdot 10^{-3}\,\Omega^{-1}$, $-1.25 \cdot 10^{-4}\,\Omega^{-1}$, $1 \cdot 10^{-3}\,\Omega^{-1}$, and $-1.25 \cdot 10^{-4}$, respectively[14], while keeping the initial conditions on memristor state and capacitor voltage unchanged as compared to the previous numerical example. As illustrated in Fig. 3(a), under $v_{u_{i,j}} = -1\,\text{V}$, as expected from rule 1, the cell state monotonically decreases toward an equilibrium $\bar{v}_{x_{i,j}} < -v_{sat}$. However, here $v_{x_{i,j}}$ evolves at all times along the respective SDR_{on} only if $n_B \leq 3$. On the contrary, differently from the previous case study, for $n_B \geq 4$ the modulus of the negative-valued offset current from equation (13) becomes so large that, at some point, the capacitor voltage decreases below $-V_t$, i.e. the negative threshold voltage for on-to-off memristor switching, proceeding along the directed off-memristor-based $\dot{v}_{x_{i,j}}$–$v_{x_{i,j}}$ locus, i.e. SDR_{off}, thereafter. As shown in Fig. 3(b), under $v_{u_{i,j}} = +1\,\text{V}$, the cell state evolves always along the on memristor-based dynamic route, as it approaches an equilibrium $\bar{v}_{x_{i,j}} < (>) - (+)v_{sat}$ for $n_B = 8$ ($n_B \leq 7$) in agreement with rule 2 (3).

[10] A M-CNN is uncoupled if $a_{k,l} = 0\,\Omega^{-1}$ for all $k,l \in \{-1,0,1\}$ except for $(k,l) = (0,0)$. A M-CNN is non-autonomous if $b_{k,l} \neq 0\,\Omega^{-1}$ for at least one (k,l) pair, with $k,l \in \{-1,0,1\}$.

[11] Given that the M-CNN is uncoupled, the cell steady-state output voltage $v_{y_{i,j}}(t_{i,j}^{(s)})$ is influenced by the dynamic behaviours of the states of the direct neighbors, only.

[12] Employing a resistor of resistance R_x in parallel to the capacitor in Fig. 1 leads to a beneficial reduction in the magnitude of the cell equilibrium $\bar{v}_{x_{i,j}}$ in all cases, ensuring to keep the electrical stress, exerted on the memristor at equilibrium, to a bare minimum.

[13] It is also possible to synthesise the EDGE M-CNN gene so that, for each cell, setting $x_{m_{i,j}}(0) = x_{off}$ and $v_{x_{i,j}} = 0\,\text{V}$, the capacitor voltage would evolve along the directed off memristor-based $\dot{v}_{x_{i,j}}$–$v_{x_{i,j}}$ locus, i.e. SDR_{off}, in each scenario of any rule.

[14] As descends from equation (12), similarly as in the previous case study, the cell is bistable for either memristor resistive state.

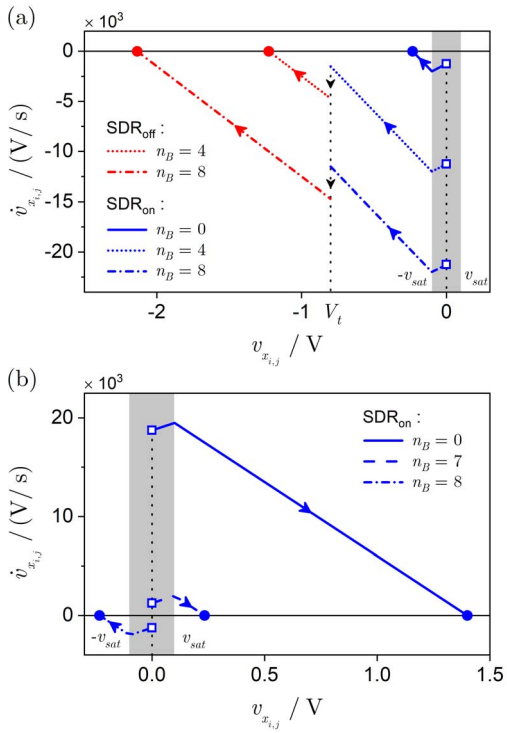

Figure 3. (a) Paths followed by the state of the cell ODE (11) toward an equilibrium, located in the negative saturation region, under $v_{u_{i,j}} = -1\,\mathrm{V}$, for some representative n_B value, specifically 0, 4, and 8. While $\bar{x}_{m_{i,j}}$ in equation (11) is fixed to x_{on} throughout the state evolution toward the respective equilibrium in case $n_B \leq 3$, it switches to x_{off} as soon as $v_{x_{i,j}}$ decreases below $-V_t$, keep unchanged thereafter, for $n_B \geq 4$. (b) Convergence of the capacitor voltage to an equilibrium in the negative (positive) saturation region along the respective SDR_{on} under $v_{x_{i,j}} = +1\,\mathrm{V}$ for $n_B = 8$ ($n_B \in \{0, 7\}$).

IV. Image Processing in Bio-Inspired Arrays with Analogue Dynamic Memristors

If the memristor undergoes smooth conductance modulation upon voltage excitation[15], the first-order cell model approximation is no longer valid. In these circumstances, a proper mathematical description for a M-CNN cell is the second-order ODE (1)-(2). As discussed in section II, a deep investigation of the nonlinear dynamics of the second-order M-CNN cell is enabled by the recently-introduced DRM_2 [10] system-theoretic technique, which is briefly reviewed below.

Remark 1: A Second-Order Dynamic Route Map DRM_2 is a family of two-dimensional graphs, each of which is associated with a particular choice of a control parameter[16]. With reference to the M-CNN cell DRM_2, one of such graphs, called State Dynamic Portrait (SDP), illustrates how the second-order ODE (1)-(2) partitions the $x_{m_{i,j}}$-$v_{x_{i,j}}$ phase plane in at most four distinct regions, differing one from the other for the sign of $\dot{x}_{m_{i,j}}$ and/or for the sign of $\dot{v}_{x_{i,j}}$, and divided by the $\dot{x}_{m_{i,j}} = 0\,\Omega \cdot \mathrm{s}^{-1}$ and $\dot{v}_{x_{i,j}} = 0\,\mathrm{V} \cdot \mathrm{s}^{-1}$ loci, which, intersecting one with the other, form the cell equilibria $\{(\bar{x}_{m_{i,j}}, \bar{v}_{x_{i,j}})\}$, as elucidated in the caption of Fig. 4. Importantly, a directed curve, drawn in blue on a cell SDP, represents a *Second-Order State Dynamic Route* (SDR_2), illustrating the path the trajectory point $(x_{m_{i,j}}, v_{x_{i,j}})$ traces over time from a given initial condition $(x_{m_{i,j}}(0), v_{x_{i,j}}(0))$.

It should be further noted that the DRM_2 is a truly general theoretical tool, allowing the analysis of any nonlinear dynamical system with two degrees of freedom, including the basic cell of the proposed M-CNN [18].

A. Binary Image Edge Extraction through a M-CNN with Analogue Dynamic Memristors

A rigorous technique [19] can be applied to the cell ODE set (1)-(2) to derive a suitable gene, allowing to shape the DRM_2 in such a way that the resulting M-CNN may accomplish the binary image edge extraction task. According to this methodology, for each scenario of any local rule from Table I, inequalities, constraining the direction of the vector field $(\dot{x}_{m_{i,j}}, \dot{v}_{x_{i,j}})$ as well as number, and local stability of the cell equilibria in the three regions of the standard output nonlinearity (9) are written down[17]. On the basis of the memory function or computing task to be implemented through a M-CNN, an analytical treatment of the cell ODE set (1)-(2) allows to set up a number of inequalities [19], which establish the existence and shape of the $\dot{v}_{x_{i,j}} = 0\,\mathrm{V} \cdot \mathrm{s}^{-1}$ loci[18], and, consequently, the number and stability properties of the equilibria on the cell SDP associated to any scenario from each local rule. In regard to the EDGE M-CNN design, inequalities[19] were written down in such a way that the cell SDP emerging for each value, which n_B may possibly assume, in rules 1 and 2 (rule 3) would accomodate a single globally asymptotically stable equilibrium in the negative (positive) saturation region. Setting $R_x = 1\,\mathrm{k}\Omega$, the values for the non-null gene parameters, specifically a_{00}, b, $b_{0,0}$, and z, obtained from the concurrent solution of the respective inequality set, respectively are: $20 \cdot 10^{-4}\,\Omega^{-1}$, $-1 \cdot 10^{-4}\,\Omega^{-1}$, $80.5 \cdot 10^{-5}\,\Omega^{-1}$, and $-1 \cdot 10^{-4}$. Inspecting the resulting cell SDPs under $v_{u_{i,j}} = -1\,\mathrm{V}$, depicted for the limiting cases $n_B = 0$ and $n_B = 8$ in plots (a), and (b) of Fig. 4, respectively, irrespective of the initial condition the cell state asymptotically converges toward an equilibrium in the negative saturation, as established by rule 1. Under $v_{u_{i,j}} = +1\,\mathrm{V}$, as clear from plot (a) ((b)) of Fig. 5, showing the cell SDP for the only case $n_B = 8$ in rule 2 (for the limiting case $n_B = 7$ in rule 3), all solutions of the ODE set (1)-(2) approach an equilibrium located in the negative (positive) saturation region, in accordance with Table I.

[15] With the capacitance of the cell capacitor fixed to $C_x = 10\,\mu\mathrm{F}$, setting $\alpha = 10^5\,\Omega \cdot \mathrm{V}^{-1} \cdot \mathrm{s}^{-1}$, and $\beta = 10^6\,\Omega \cdot \mathrm{V}^{-1} \cdot \mathrm{s}^{-1}$ in the formula of equation (5) for $k(v_{x_{i,j}})$, the time evolution of the cell state $v_{x_{i,j}}$ finely tunes the memristor resistance [10].

[16] For the case of the M-CNN second-order cell, the control parameter may be $a_{0,0}$, or $i_{w_{i,j}}$.

[17] The solution of the inequality set may be optimized to ensure that phase plane trajectories, starting off from pre-defined initial conditions, keep clear of the boundaries of the basins of attraction of the equilibria they are expected to converge to as time approaches infinity [19].

[18] It can be shown that, for the memristor model under consideration, the shape of the $\dot{x}_{m_{i,j}} = 0\,\Omega \cdot \mathrm{s}^{-1}$ loci may not be massaged through ad-hoc inequalities. Thus, for the particular cell model under study, our SDP synthesis method [19] may only arrange the number and properties of the $v_{x_{i,j}}$ nullclines.

[19] For the details of the EDGE M-CNN design procedure, the reader is invited to consult [19].

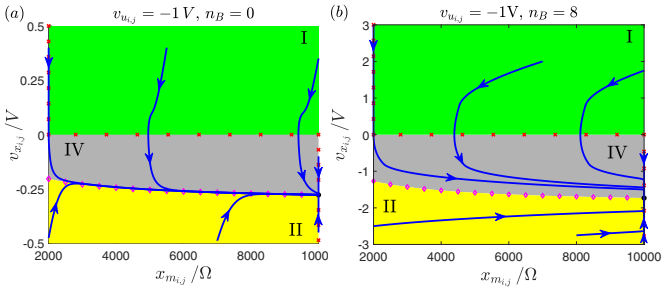

Figure 4. (a) ((b)): Binary image edge extraction M-CNN cell SDP under $v_{u_{i,j}} = -1\,\text{V}$ for $n_B = 0$ ($n_B = 8$). Here $v_{y_{i,j}}(t^s_{i,j}) = -v_{sat}$, as requested by rule 1. Green region I: $\dot{v}_{x_{i,j}} < 0\,\text{V/s}$ and $\dot{x}_{m_{i,j}} < 0\,\Omega\text{/s}$. Yellow region II: $\dot{v}_{x_{i,j}} > 0\,\text{V/s}$ and $\dot{x}_{m_{i,j}} > 0\,\Omega\text{/s}$. Cyan region III: $\dot{v}_{x_{i,j}} > 0\,\text{V/s}$ and $\dot{x}_{m_{i,j}} < 0\,\Omega\text{/s}$. Grey region IV: $\dot{v}_{x_{i,j}} < 0\,\text{V/s}$ and $\dot{x}_{m_{i,j}} > 0\,\Omega\text{/s}$. Red crosses: $\dot{x}_{m_{i,j}} = 0\Omega\text{/s}$. Magenta diamonds: $\dot{v}_{x_{i,j}} = 0\,\text{V/s}$. Black circles: $\dot{v}_{x_{i,j}} = 0\,\text{V/s}$ and $\dot{x}_{m_{i,j}} = 0\,\Omega\text{/s}$. A filled circle signifies the stability of the respective equilibrium. Blue curves: phase-plane trajectories from numerical simulation of equations (1)-(2).

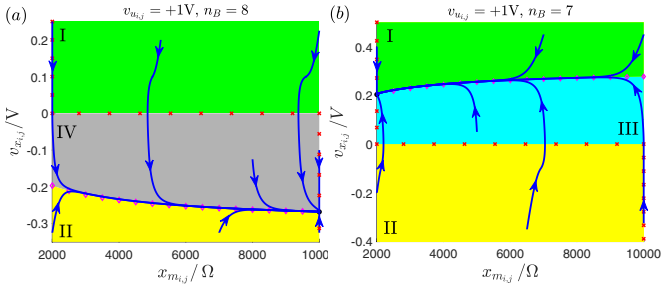

Figure 5. (a) ((b)): Binary image edge extraction M-CNN cell SDP under $v_{u_{i,j}} = +1\,\text{V}$ for $n_B = 8$ ($n_B = 7$). In the first (latter) case $v_{y_{i,j}}(t^s_{i,j}) = -(+)\,v_{sat}$, as established by rule 2 (3).

V. Conclusions

One of the most significant add-on functionality, which memristors may endow CNNs with, is the programmability of the cells, traditionally used merely as data processing units, to implement read and write memory access operations without additional circuitry. This will allow to increase considerably the spatial resolution of state-of-the-art CNN Universal Machines, which currently accommodate spacious data storage units in each processing element so as to endow the technical system with local stored programmability on board. Moreover, in comparison to classical CNNs, the memristive variants may support a wider spectrum of dynamical behaviours, which are induced by the inherently-high degree of nonlinearity of the switching kinetics of memristors, and allow the development of innovative forms of computing, which promise to outperform the conventional signal processing paradigm. In order to offer a glimpse on the principles of the M-CNN computing paradigm, and on its potential to enrich the panorama of functionalities featured by standard cellular arrays, the classical DRM analysis tool or its recent generalization for second-order dynamical systems is applied to the model of each cell in a memristive variant of a standard space-invariant CNN with bistable-like or analog dynamic memristors in each processing element, respectively, to elucidate the mechanisms by which the memristive bio-inspired cellular structure accomplishes a fundamental image processing task.

Acknowledgements

This work was financially supported by the Czech Science Foundation (GACR) through the grant no. 18-21608S.

References

[1] L. Chua, and T. Roska, "Cellular Neural Networks and Visual Computing: Foundations and Applications," 1st edition, Cambridge University Press, 2002

[2] A.R. Vázquez, J. Fernández-Berni, J. A. Leñero-Bardallo, I. Vornicu, and R. Carmona-Galán, "CMOS Vision Sensors: Embedding Computer Vision at Imaging Front-Ends," *IEEE Circuits and Systems Magazine*, vol. 18, no. 2, pp. 90–107, 2018, DOI: 10.1109/MCAS.2018.2821772

[3] I. Tzouvadaki, G. De Micheli, and S. Carrara, "Memristive Biosensors for Ultrasensitive Diagnostics and Therapeutics," in *Applications of Emerging Memory Technology Beyond Storage*, M. Suri ed., Springer Series in Advanced Microelectronics, pp. 133–157, 2020, ISBN-13: 978-981-13-8378-6

[4] Z. Sun, G. Pedretti, E. Ambrosi, A. Bricalli, W. Wang, and D. Ielmini, "Solving matrix equations in one step with cross-point resistive arrays," *Proceedings of the National Academy of Sciences of the United States of America (PNAS)*, vol. 116, no. 10, pp. 4123–4128, 2019

[5] L. Nicolosi, A. Blug, F. Abt, R. Tetzlaff, H. Höfler, and D. Carl "Real time control of laser beam welding processes: Reality. Focal-plane sensor-processor chips", A. Zárandy ed., Springer, pp. 261–282, 2011, ISBN: 978-1-4419-6474-8

[6] T. Roska, "The CNN universal machine: an analogic array computer," *IEEE Transactions on Circuits and Systems–II: Analog and Digital Signal Processing*, vol. 40, no. 3, pp. 163–173, 1993

[7] D. Ielmini, and R. Waser, "Resistive Switching: From Fundamentals of Nanoionic Redox Processes to Memristive Device Applications," *Wiley-VCH*, 1st edition, 2016, ISBN-13: 978-3527334179

[8] L.O. Chua, "5 Non-Volatile Memristor Enigmas Solved," *Applied Physics A*, vol. 124, 563(43pp.), 2018

[9] L.O. Chua, "Everything you wish to know about memristors but are afraid to ask," *Radioeng.*, vol. 24, no. 2, pp. 319–368, June 2015

[10] R. Tetzlaff, A. Ascoli, I. Messaris, and L.O. Chua, "Theoretical Foundations of Memristor Cellular Nonlinear Networks: Memcomputing with Bistable-like Memristors," *IEEE Trans. on Circuits and Systems–I: Regular Papers*, 2019, DOI: 10.1109/TCSI.2019.2940909

[11] L.O. Chua, "If It's Pinched, It's a Memristor," *Semiconductor Science and Technology*, Special Issue on Memristive Devices, vol. 29, no. 10, (42 pp.), 2014

[12] Y.V. Pershin, and M. Di Ventra, "Memory effects in complex materials and nanoscale systems," *Advances in Physics*, vol. 60, no. 2, pp. 145–227, 2011

[13] S.H. Jo, K.-H. Kim, and W. Lu, "High-Density Crossbar Arrays Based on a Si Memristive System," *Nano Lett.*, vol. 9 , no. 2, pp. 870–874, 2009

[14] Z. Biolek, D. Biolek, and V. Biolková, "Spice model of memristor with nonlinear dopant drift," *Radioeng.*, vol. 18, no. 2, pp. 210–214, 2009

[15] S. Duan, X. Hu, Z. Dong, L. Wang, and P. Mazumder, "Memristor-Based Cellular Nonlinear/Neural Network: Design, Analysis, and Applications," *IEEE Trans. on Neural Networks and Learning Systems*, vol. 26, no. 6, pp. 1202–1213, 2015

[16] M. Di Marco, M. Forti, and L. Pancioni, "Complete stability of feedback CNNs with dynamic memristors and second-order cells," *Int. J. Circuit Theory Appl.*, vol. 44, pp. 1959–1981, Nov. 2016

[17] M. Di Marco, M. Forti, and L. Pancioni, "Convergence and multistability of nonsymmetric cellular neural networks with memristors," *IEEE Trans. Cybern.*, vol. 47, no. 10, pp. 2970–2983, Oct. 2017

[18] A. Ascoli, I. Messaris, R. Tetzlaff, and L.O. Chua, "Theoretical Foundations of Memristor Cellular Nonlinear Networks: Stability Analysis with Dynamic Memristors," *IEEE Trans. on Circuits and Systems–I: Regular Papers*, 2019, DOI: 10.1109/TCSI.2019.2957813

[19] A. Ascoli, R. Tetzlaff, S.M. "Steve" Kang, and L.O. Chua, "Theoretical Foundations of Memristor Cellular Nonlinear Networks: A DRM_2-based Method to Design Memcomputers with Dynamic Memristors," *IEEE Trans. on Circuits and Systems–I: Regular Papers*, 2020, DOI: 10.1109/TCSI.2020.2978460